Title

New emissive mononuclear copper (I) complex: Structural and photophysical characterization focusing on solvatochromism, rigidochromism and oxygen sensing in mesoporous solid matrix

Authors

Ravaro, Leandro P
Mafud, Ana C
Li, Zhi
et al.

Publication Date

2018-12-01

DOI

10.1016/j.dyepig.2018.07.020

New emissive mononuclear copper (I) complex: Structural and photophysical characterization focusing on solvatochromism, rigidochromism and oxygen sensing in mesoporous solid matrix

Leandro P. Ravaro[a,b*], Ana C. Mafud[a], Zhi Li[b], Eric Reinheimer[c], Carlos A. Simone[a], Yvonne P. Mascarenhas[a], Peter C. Ford[b] and Andrea S. S. de Camargo[a*]

[a]São Carlos Institute of Physics, University of São Paulo, PO Box 369, 13560-970, São Carlos, SP, Brazil

[b]University of California Santa Barbara, Santa Barbara, CA 93106, U.S.

[c]Rigaku Americas

ABSTRACT

We report the structural and photophysical property analyses of a new emissive copper (I) complex $CuI(PPh_3)(L)$ (**1**, L = 4,4'-dimethoxy-2,2'-bipyridine) which demonstrates solvatochromism. When recrystallized from acetonitrile, the originally orange color of **1** becomes yellow and demonstrates a blue-shifted, broad emission spectrum. This process is reversed when the yellow solid is redissolved in dichloromethane and recrystallized. The lattice parameters and angles found were *a* = 17.769 Å, β = 114.05 ^{o} and *a* = 11.555 Å, angle β = 92.70 ^{o} for the orange and yellow forms of **1**, respectively, and there are notable structure differences for $CuI(PPh_3)(L)$ in these two solids. When loaded into a mesoporous silica, the emission blue shift becomes greater, indicating a strong rigidochromic effect at room temperature. The emission from such copper complex loaded mesoporous silica matrix is quenched by oxygen and this quenching has been quantified.

1. INTRODUCTION

Metallo-organic complexes based on 3d-block transition metals have potential technological applications due to their low cost compared to other noble metals [1-5]. In particular, copper(I) complexes have tunable emission properties that can be modulated throughout the visible spectrum depending on the ligand coordinated to the copper(I) center [6,7]. Furthermore, multinuclear Cu(I) complexes [8,9] present photophysical properties different from those of mononuclear complexes [10,11]. Common applications for Cu(I) complexes include OLEDs [12-15], catalysts [16-18], bio-images [19-21], gas sensors [22-25], vapochromic sensors [26-29], and solvatochromic sensors [30,31]. For the two lattermost applications, the compounds exhibit color changes and, in some cases, changes in emission properties when exposed to vapors of volatile organic compounds (VOCs) [32-37]. Such effects are often the result of structural changes in the metal center coordination distances and corresponding metal-metal and ligand-metal interactions [38-41].

Certain copper(I) solids have been studied for their applicability to gas sensor devices, especially for dioxygen, as their luminescence is quenched when exposed to O_2 [42,43]. These material have free access channels (void spaces) in their crystal structures where O_2 molecules can reside and quench excited states [43,44]. Some emitting complexes become more amenable to gas sensing when incorporated into porous solid matrices. The pores provide the sensor molecules a greater degree of dispersion and greater contact surface that increase interactions between the gas and emitting molecule [45]. However, when the emitting metallo-organic complexes are hosted in a more rigid environment, their emission spectra may be shifted owing to excited state distortions from the ground states, a phenomenon known as the “rigidochromic effect” [46-49].

In this work, we report the structural and photophysical properties of a new emissive copper(I) complex $CuI(PPh_3)(L)$ (**1**, L = 4,4'-dimethoxy-2,2'-bipyridine), the absorption and emission spectra of which demonstrate solvatochromism and rigidochromism as well as sensitivity to O_2 by luminescence quenching when loaded in mesoporous silica. When recrystallized from acetonitrile, the originally orange complex changes color to yellow while its broad emission spectrum is shifted to the blue. This process is reversible when the yellow form is recrystallized from dichloromethane.

According to X-Ray analysis, the yellow form has acetonitrile molecules in its crystalline structure interacting with the 4,4'-dimethoxy-2,2'-bipyridine and triphenylphosphine ligands. Both crystals are monoclinic, but with different lattice parameters. The yellow color is also maintained in acetonitrile solution, indicating that the solvatochromic effect is probably due a supramolecular interaction between the acetonitrile and the aromatic ligands [30,31]. In this context, the x-ray crystallographic results may provide insight into interactions between solvent and complex the lead to solvatochromic effects. When **1** is loaded in solid mesoporous silica matrix there is a blue-shift in the emission spectrum indicating a rigidochromic effect. Additionally, this emission is sensitive to O_2 quenching by oxygen, suggesting that this hybrid material can serve as a luminescent oxygen sensor.

2. EXPERIMENTAL SECTION

2.1 Synthesis of the copper(I) complexes

[CuI(PPh_3)(L)] (**1**), L = 4,4'-dimethoxy-2,2'-bipyridine). To achieve the synthesis of **1**, CuI (1 mmol, 98% from Sigma-Aldrich) was dissolved in dichloromethane (DCM, 10 mL) with magnetic stirring under a nitrogen atmosphere until complete dissolution of the CuI. Immediately after dissolution, the ligands 4,4'-dimethoxy-2,2'-bipyridine (L) (1 mmol, 97% from Sigma-Aldrich) and triphenylphosphine (PPh_3, 1 mmol, 99% from Sigma-Aldrich) were added and the mixture was stirred under flowing nitrogen for 2 h in the dark. After this, the resulting orange precipitate was collected by filtration and dried under constant flow of N_2 for 48 h. The yield was 75%. ^{1}H NMR spectrum (500 MHz, CD3COCD3) δ ppm 4.02 (s, 6H) 7.30-7.37 (m, 6H) 7.38-7.43 (m, 3H) 7.44-7.50 (t, 6H) 7.52-7.57 (m, 2H) 7.60-7.65 (m, 2H) 7.67-7.72 (m, 2H). IR (ATR): ν = 493 (m), 503 (m), 523 (vs), 540 (w), 574 (vw), 590 (vw), 694 (vs), 722 (w), 747 (m), 820 (w), 830 (w), 845 (vw), 863 (w), 881 (vw), 900 (vw), 914 (vw), 998 (vw), 1023 (s), 1044 (w), 1091 (vw), 1120 (vw), 1157 (vw), 1180 (vw), 1215 (m), 1248 (m), 1270 (w), 1308 (w), 1325 (w), 1409 (w), 1422 (w), 1431 (w), 1454 (vw), 1467 (vw), 1478 (vw), 1490 (w), 1560 (m), 1604 (m), 2833 (vw), 2941 (vw), 2973 (vw), 2994 (vw), 3022 (vw), 3050 (vw), 3068 (vw). Anal. for $C_{30}H_{27}CuIN_2O_2P$ (668.94): C 53.78, H 4.21, N 4.18; found C 53.13, H 4.19, N 4.15.

[CuI(PPh_3)(L)] (1-ACN**).** To obtain this solid, complex **1** was dissolved in acetonitrile (ACN) and the solvent was slowly removed under nitrogen flow for 1 week.

[CuI(PPh$_3$)(L)]-SiO$_2$ (1-@SiO$_2$**).** Mesoporous silica was prepared as previously reported [45], and the loading of **1** into the pores of the silica matrix was accomplished using wet impregnation. In order to achieve this, 300 mg of powdered mesoporous silica were added to a solution of **1** (1.0 mM) prepared with 10 mL acetone. The heterogeneous mixture was stirred at 120 Hz for a period of 24 h, after which the solvent was removed by filtration, and the matrix impregnated with the copper complex was dried in vacuum and under N_2 flow for 1 week. For simplicity, the material prepared by incorporating **1** into SiO_2 was designated as **1**@SiO_2.

2.2 Instrumentation and Measurements:

Liquid-state NMR measurements were completed using an Agilent Technologies 500/54 Premium Shielded NMR Spectrometer operating at 500 MHz (^{1}H). The reference standard for ^{1}H chemical shifts was tetramethylsilane (TMS), and all samples were dissolved in deuterated acetone. X-ray fluorescence measurements were done with an Ag filter using a PANalytical MiniPal 4 spectrometer operating at the power 30 kV and 300 µA. FTIR measurements were performed by the Attenuated Total Reflection (ATR) technique using a PerkinElmer model Spectrum Two spectrometer. Electronic absorption spectra were acquired on a Shimadzu UV-2401PC UV-Visible spectrophotometer. The photoluminescence (PL), photoexcitation (PE) and quantum yield (QY) measurements were done using a Horiba model Fluorolog FL-1057 fluorimeter coupled to Quanta–φ integrating sphere. The excited state lifetime measurements were performed using Time-Correlated Single Photon Counting (TCSPC) technique.[50] Approximately 100 femtosecond (fs) excitation pulses with wavelength 400 nm were generated by doubling the fundamental frequency of fs from a Ti:Sapphire laser (SpectraPhysics Tsunami) with an optical harmonic generator (Inrad). The laser repetition rate was reduced to 2 MHz by a home-made acousto-optical pulse picker in order to avoid saturation of the chromophore. The TCSPC system is equipped with thermoelectrically-cooled single-photon counting avalanche photodiode (Micro Photon Devices) and electronics board (Becker & Hickl SPC-630) and has an instrument response time about 30-40 picoseconds. The triggering signal for the TCSPC board was generated by sending a small fraction of the laser beam onto a fast (400 MHz bandwidth) Si photodiode (Thorlabs Inc.). The fluorescence signal was dispersed by an Acton Research

SPC-500 monochromator after passing through a pump blocking, long wavelength-pass, autofluorescence-free, interference filter (Omega Filters, ALP series). In addition to the time-resolved detector, the monochromator is equipped with a CCD camera (Roper Scientific PIXIS-400) allowing for monitoring of the time-averaged fluorescence spectrum. Luminescence transients were not deconvoluted from the instrument response function since their characteristic time-constants were much longer than the system response to the excitation pulse.

Measurements of luminescence quenching as a function of oxygen exposure were done using an in-house apparatus that provided a controlled release of an O_2/N_2 (99.999%) mixture at variable molar fractions of O_2 ranging from 0.0 to 1.0 at 1.0 atm. Total. The gas lines were connected by two dual stage low-pressure valves from CONCOA each having a maximum output pressure of 15 psi and two low-flow rotameters (0-1000 ml/min). Crystallographic data for the compounds were collected on a Bruker APEX II diffractometer furnished with a Kryoflex II liquid N_2 cryogenic cooling system and graphite-monochromated MoKα (0.71073 Å at 291 K) radiation with ω-2θ scan technique. Data collection was completed using the APEX II program (Apex II, Bruker AXS: Bruker Suite, version 2008/3; Bruker AXS Inc.: Madison, WI, USA, 2008). Indexing, frame integration, Lorentz-polarization corrections and final cell parameter calculations were completed using CrysAlis^{Pro} software. Multi-scan absorption corrections were performed using the SCALE3 ABSPACK algorithm which was integrated into CrysAlis^{Pro}. The crystal structure was solved via intrinsic phasing using ShelXT and refined using ShelXL within the Olex2 graphical user interface. The structural model's space group was unambiguously verified by PLATON. The hydrogen atom positions bounded to oxygen atoms were located in the difference Fourier map and refined with U*iso*(H) = 1.5 U*eq*(O). The C-bound H-atoms of the anion were included in calculated positions and treated as riding-model approximation: C–H = 0.97 Å, with U*iso*(H) = 1.2 U*eq* (parent C-atom) and allowed to ride on the parent carbon atoms.

Differential scanning calorimetry (DSC) and thermal gravimetric analysis (TGA) were used to determine the thermal mass loss, as well as to study the thermal decomposition. Thermal analyses of the purified samples were performed using simultaneous differential thermal analysis (DTA) and thermogravimetry (TG), SDT 2960 - TA Instruments, at a heating rate of 10 °C/min, in a flow of nitrogen, from room

temperature to 600 °C. DSC/TGA and DSC analysis were carried out with an initial sample mass of 5.0 mg in aluminum pans.

3. RESULTS AND DISCUSSION

3.1 Solvatochromism of [CuI(PPh_3)(4,4'-dimethoxy-2,2'-bipyridine)] (1).

The change in the color of some molecules depending on the polarity of the solvent is known as solvatochromism [51,52]. When compound **1** is dissolved in ACN a slightly yellow-colored solution is obtained while the color is distinctly orange when dissolved in DCM owing to distinct changes in the visible spectrum (λ > 400 nm) as shown in Figure 1. Solutions of **1** also exhibit intense UV absorptions between 200-300 nm, attributed to ligand centered π-π* transitions that shift to the blue as a function of increasing solvent dipole moment (D) according to the order $CHCl_3$ < DCM < ACN. The solvent sensitive, relatively weak bands in the visible are likely due to a metal-to-ligand charge transfer (MLCT) transition [53].

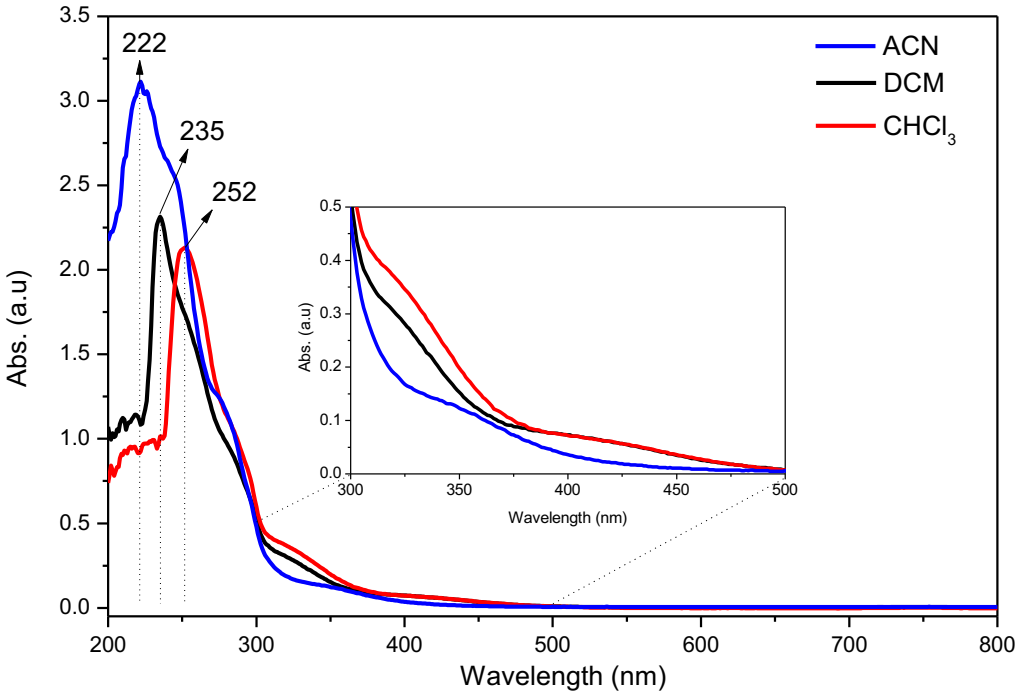

Figure 1. Optical absorption spectrum Uv-Vis for compound **1** in three different solvents with concentration ≅ 0.1 mM. Decreasing order of solvent polarity: ACN > DCM > $CHCl_3$.

These color changes carry over to the solids isolated from the DCM (orange) or ACN (yellow) as illustrated in Figure 2. However, the change from yellow to orange is a reversible process. Adding solvent (ACN) to the orange powder **1**, initiates a rapid change of color to yellow. When DCM is added to the yellow powder **1**-ACN recovered drying the ACN solution, the powder returns to its original color (orange). Notably, both forms are relatively stable, since, neither material demonstrated a color change when subjected to heating at 100 ^{o}C under vacuum.

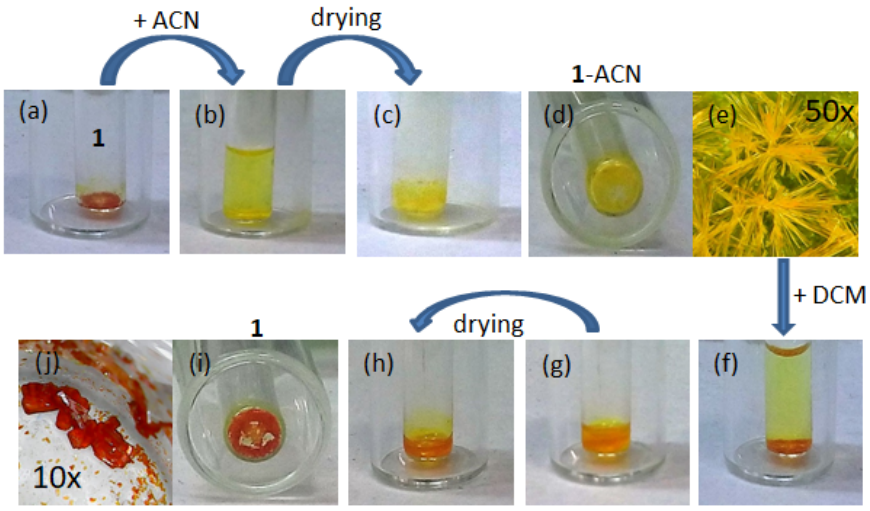

Figure 2. (a): Color change from orange to yellow for **1** after exposure to ACN (**1**-ACN). In image (i) is seen the change in color from yellow to orange on exposure of **1**-ACN to DCM, indicative of **1**. Images (e) and (j) show crystalline samples of **1**-ACN and **1** at 50x and 10x magnification, respectively, after recrystallization.

3.2 Structural and thermal characterizations

The crystal structure, chemical composition and stoichiometry of compound **1** were determined by X-ray diffraction experiments (XRD), FTIR (ATR), (^{1}H NMR), (^{31}P NMR), X-ray fluorescence (XRF) and thermal analysis (TG/DSC). Single crystals of **1** and **1**-ACN were obtained by slow evaporation of a solution of compound **1** dissolved in dichloromethane and acetonitrile, respectively and the x-ray data for the structures of these two crystals are given in Table 1. As shown in Figure 2, the appearances of the crystals for **1** and **1**-ACN are clearly different.

Table 1. Crystallographic data for Complex **1** and **1**-ACN.

Sample	**1**	**1**-ACN
Formula	$C_{30}H_{27}CuIN_2O_2P$	$C_{30}H_{27}CuIN_2O_2P$
Crystal system	Monoclinic	Monoclinic
Space group	P1 $2_1/n$ (14)	P1 $21/_C$ (14)
a(Å)	17.7698(15)	11.555(5)
b(Å)	9.1737(6)	13.800(5)
c (Å)	18.928(19)	19.705(5)
β (°)	114.057(11)	92.737(5)
Cell volume (Å³)	2817.62(50)	3138.56(19)
Crystal density (g cm^{-1})	1.58	1.50
Z	4	4
Color	Orange	Yellow

Compound **1** crystallized from dichloromethane in the centrosymmetric monoclinic space group $P2_1/n$ with a single molecule of the copper complex as asymmetric unit. The monovalent copper center exists in a distorted pseudo-tetrahedral environment (Figure 3). However, the N(1)-Cu-N(2) bite angle of the chelating, functionalized bipyridine ligand was only 78.50(5)°, similar to other complexes involving the binding of similar bis-chelating nitrogen-containing ligands, while the angles N(1)-Cu(1)-P(1) and N(2)-Cu(1)- P(1) were 132.09(11)° and 120.02(11)°, respectively, showing large distortions from tetrahedral angles (~109.5°). This observation may reflect steric effects owing to size of the iodide ions coordinated to the Cu(I) core.

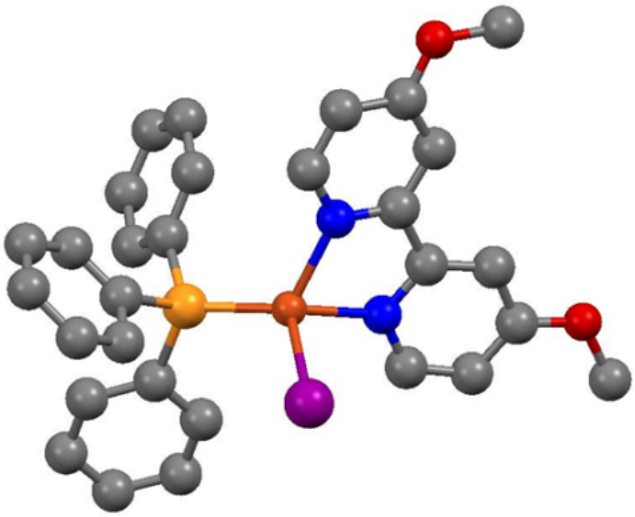

Figure 3. Structure of compound **1.** Blue: N; Yellow: P; Red: O; Violet: I; Orange: Cu and Grey: C.

The structure of **1**-ACN, which crystallized in the centrosymmetric monoclinic space group $P2_1/c$, indicates the presence of an interstitial acetonitrile molecule within the asymmetric unit (Figure 4). While the monovalent copper in **1**-ACN also exhibits a distorted tetrahedral coordination several bond angles are considerably different from those seen for the structure of **1**. These differences are compared in Figure 4. Thus, the N(1)-Cu(1)-P(1) angle in **1**-ACN was 105.41(10)°, contracted more than 26 ° from that seen in **1**, and the N(2)-Cu(1)-P(1) angle at 110.0(1)° was only slightly greater than the predicted tetrahedral geometry. As expected, the bite angle of the chelating, bipyridine ligand in **1**-ACN was 78.70(12)°, a value close to that in **1,** while the P(1)–Cu(1)–I(1), N(1)–Cu(1)–I(1) and N(2)–Cu(1)–I(1) increased by 10.97, 15.35 and 6.73°, respectively, in going from **1** to **1**-ACN. Closer analysis of the conical arrangement of phenyl rings bound to the phosphorus atom within the copper complex of **1**-ACN demonstrated that even though the angles around the phosphorus are contracted from those predicted for a tetrahedron, they are not contracted to the same extent as those for **1**. Unlike **1**, where no supramolecular interactions existed between neighboring molecules, closer structural analysis of neighboring molecules within the structure of **1**-ACN, revealed the presence of an inversion center in the void space between neighboring chelating bipyridine ligands (Figure 5). This not only relates two copper complex molecules by symmetry, but also influences π-π interactions between the adjacent aromatic rings as evidenced by centroid-to-centroid distances of 3.5427(14) Å between the rings. The

observed distortions change the molecular packing resulting in a larger unit cell volume and lower overall density. These changes are the most likely factors responsible for the color change and the blue-shift observed in the emission spectrum.

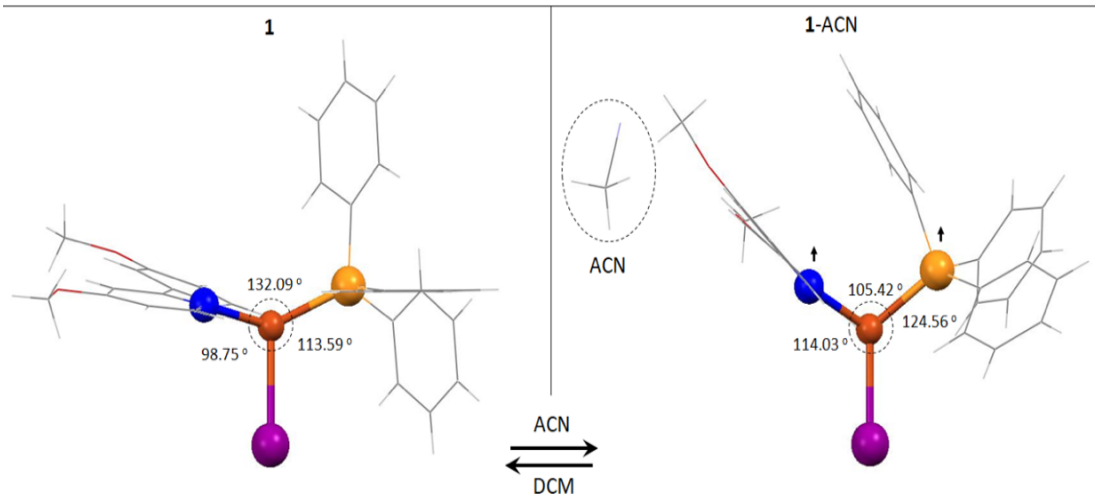

Figure 4. Comparison of the structures of **1** and **1**-ACN showing bond angles before and after recrystallization from ACN.

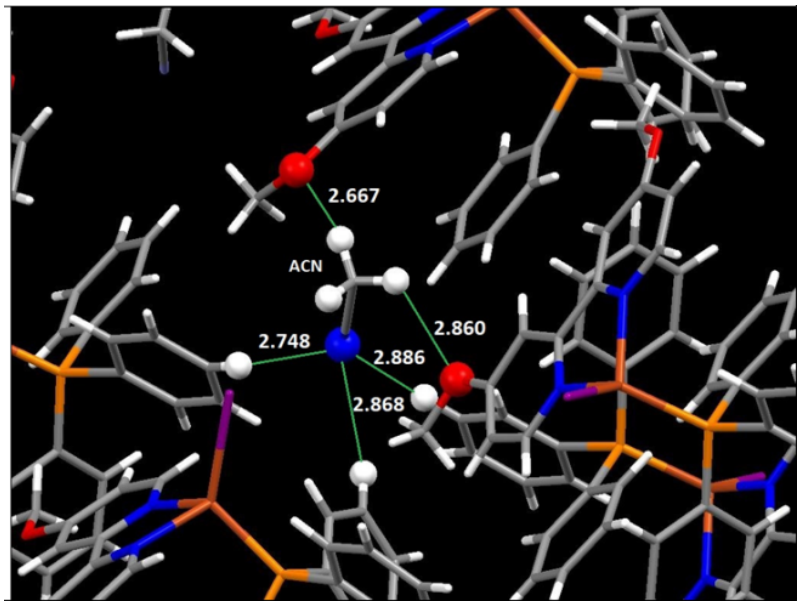

Figure 5. interaction of the ACN with the surrounding ligands in the structure of **1**-ACN. Blue: N; Yellow: P; Red: O; Violet: I; Orange: Cu; Grey: C and White: H.

Table 2 summarizes key bond lengths and angles found for the crystal structures of **1** and **1**-ACN.

Table 2. Bond lengths and angles between atoms for compounds **1** and **1**-ACN

Sample	Distance	(Å)	Angle	(°)
1	Cu(1)-I(1)	2.6592(7)	P(1)-Cu(1)-I(1)	113.59(4)
	Cu(1)-P(1)	2.1985(14)	N(1)-Cu(1)-I(1)	98.74(10)
	Cu(1)-N(1)	2.073 (4)	N(2)-Cu(1)-I(1)	107.80(11)
	Cu(1)-N(2)	2.101(4)	N(1)-Cu(1)-P(1)	132.09(11)
			N(2)-Cu(1)-P(1)	120.02(11)
			N(1)-Cu(1)-N(2)	78.50(15)
1-ACN	Cu(1)-I(1)	2.5562(8)	P(1)-Cu(1)-I(1)	124.56(4)
	Cu(1)-P(1)	2.2100(13)	N(1)-Cu(1)-I(1)	114.09(9)
	Cu(1)-N(1)	2.083 (3)	N(2)-Cu(1)-I(1)	114.53(9)
	Cu(1)-N(2)	2.083(13)	N(1)-Cu(1)-P(1)	105.41(9)
			N(2)-Cu(1)-P(1)	110.0(1)
			N(1)-Cu(1)-N(2)	78.70(12)

Thermal gravimetric analysis (TGA) of **1** (Supporting Information Figure S1) demonstrates significant mass losses as a function of increasing temperature. The first mass loss occurs at 175-310 °C and can be attributed to decomposition of the ligands 4-4'-dimethoxy-2-2'-bipyridine and triphenylphosphine with simultaneous generation of CuI. This mass loss is accompanied by an endothermic peak at 210 °C on the DSC curve. The theoretical value calculated for this mass loss was 72% but the experimental value was 55%; the 17% difference is attributed to the formation of an organic residue owing to incomplete degradation of the ligands. Figure S1, also shows a second mass loss at (310-440 °C) that may be related to the removal of these organic residues. Moreover, this second weight loss is accompanied by an exothermic peak at 440 °C on the DSC curve, most likely associated with the formation of a CuI(s) crystalline phase. Thus, considering that complete formation of solid CuI (s) occurs around 440 °C, the experimentally measured weight loss of ~70% is in good agreement with that calculated (~72%). The third mass loss (440-700 °C) is related to the oxidation of CuI to CuO, an event accompanied by a weight loss of 22%. The total experimental weight lost by **1** (92%) is in good agreement with the theoretical value (~90%) for this series of events.

3.3 Photophysical characterization

The excitation and photoluminescence spectra for solid **1**-ACN at 298 K and 77 K can be seen in Figure 6. At 298 K, the powder has a broad band emission with a maximum λ_{max}^{PL} at 668 nm exciting at λ_{exc} = 420 nm. The PL quantum yield (Φ_{PL}) measured under these conditions was 0.18. This broad luminescence is characteristic of metal (Cu(I)-to-ligand (bipyridine) charge transfer (MLCT) excited states with possibly some contribution from the iodide (i.e. (M+I)LCT) [29,54]. At 77 K, the emission maximum for the solid is red-shifted to 696 nm, a difference of 28 nm with respect to the emission spectrum at 298 K. For solid **1** (shown in S9) the maximum emission observed was 705 nm and 716 nm in 298 K and 77 K, respectively. No emission was observed for **1** when dissolved acetonitrile or dichloromethane solution at room temperature. As reported earlier [54-57], the lack of an emissive response from some copper (I) halide complexes is commonplace due to chemical instability toward partial ligand dissociation, dimerization, etc.

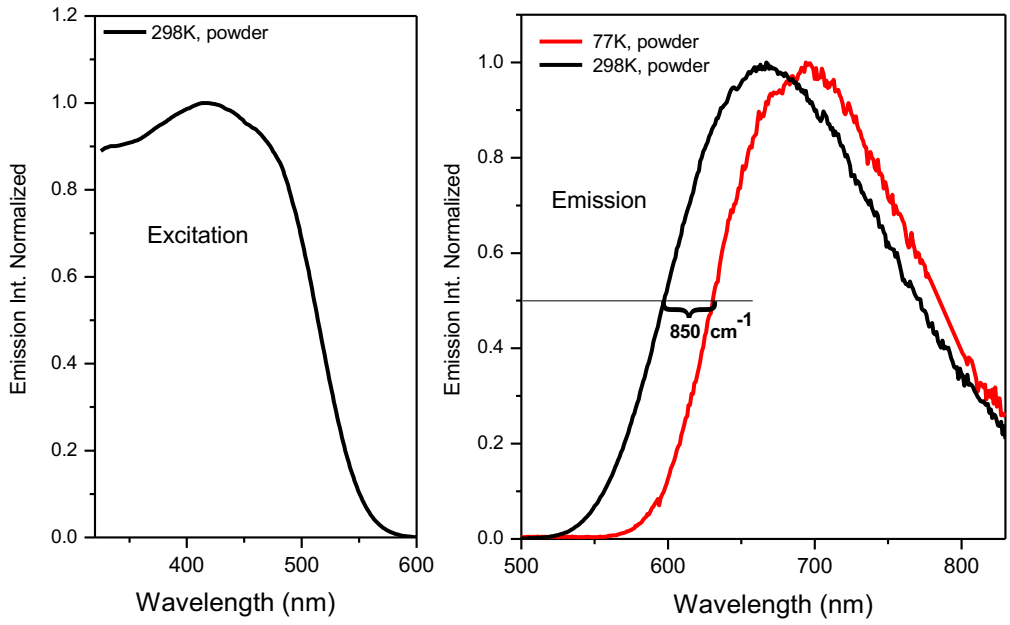

Figure 6. *Left:* Excitation spectra for **1**-ACN powder at room temperature monitored at its emission maximum at 668 nm. *Right:* Emission spectra from powder samples of **1**-ACN at room temperature and at 77 K (λ_{exc} = 420 nm).

There is also a distinct difference between the emission spectra of the yellow solid **1**-ACN and the orange solid **1**. The PL from the latter displays a λ_{max}^{PL} at 705 nm red-shifted from that of **1**-ACN by 37 nm (Figure 7). The emission from **1** was sufficiently weak that a quantum yield could not be measured. The emission lifetimes measured for powders of **1**-ACN and 1 at room temperature were 172 and 144 ns, respectively. The red-shifted emission at 77 K may reflect a greater contribution from the triplet excited state (T_1), since the emission at room temperature with short lifetime (order of ns) may have large contribution of the singlet excited state (S_1) possibly due to the process known as thermally activated delayed fluorescence process (TADF) [58-61]. If the emission at 77 K is largely triplet in character while that at 298 K is mostly singlet, the energy separation ΔE (S_1-T_1) = 850 cm^{-1} in good agreement with other Cu(I) complexes that present the TADF effect [51,52,62].

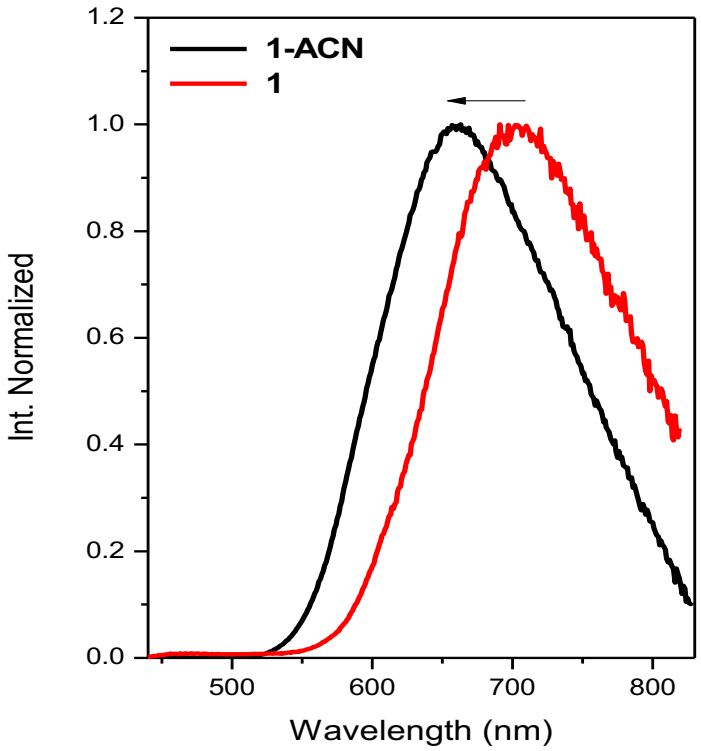

Figure 7. Normalized emission spectra (λ_{exc} = 420 nm) for powders of **1** (red) and **1**-ACN (black) at room temperature.

3.4 Rigidochromism

When **1** was loaded into silica (**1**@SiO_2), the resulting PL was a broad band with a λ_{max}^{PL} at 556 nm, substantially blue-shifted relative to that from powder sample of **1** (Figure 8). This response may be attributed to rigidochromic effects [45-48] owing to distortions of the excited state relative to the ground state. Elevated rigidity within the molecule's second coordination sphere leads to concomitant increase in the energy level of the emitting state and a blue shift of the emission maximum. Similar rigidochromic effects have been reported for the emission spectra of copper(I) clusters [9,45] and from rhenium(I) complexes displaying of MLCT electronic transitions [47,48].

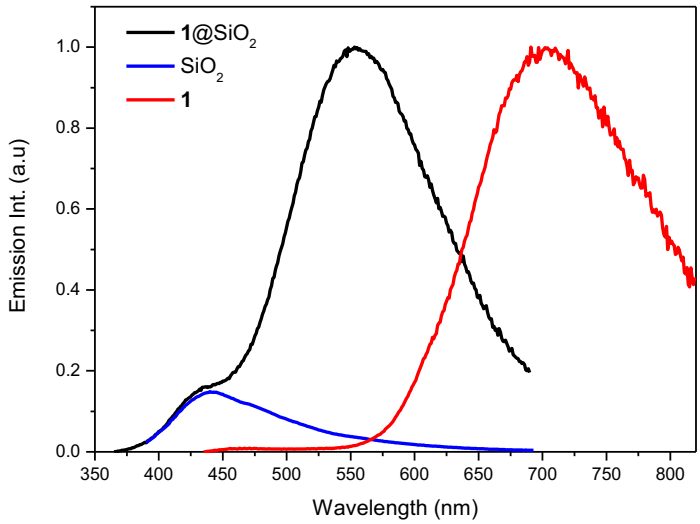

Figure 8. Emission spectra at 298 K for **1** powder (λ_{exc} = 420 nm) and for **1**@SiO_2 (λ_{exc} = 350 nm). The blue curve denotes a small contribution of a weak emission band at ~435 nm attributed to the SiO_2 matrix. This sample of **1**@SiO2 was prepared by infusing mesoporous silica with a 10^{-3} M solution of **1** in acetone. There was no qualitative difference in the emission maxima when solutions of significantly higher or lower concentration were used for the wet impregnation procedure.

According to the X-ray diffraction results the **1**@SiO_2 sample is completely amorphous (Figure S10), without crystalline structure, indicating that the copper (I) complex is highly dispersed in the silica matrix. It was also possible to verify the morphology by scanning electron microscope (SEM) images, where it is possible to see the homogeneous matrix's pores (Figure S11).

3.5 Sensitivity to dioxygen

In addition to the rigidochromic effect, **1**@SiO_2 demonstrated sensitivity to O_2. The intense PL band seen at ~560 nm under a continuous flow of N_2 is largely quenched under a continuous flow of pure O_2 (0.92 atm). Upon exposure to increasing oxygen concentrations, the steady state PL intensity decreases by a factor of ~8 as seen in Figure 10. This process is reversible, flushing with N_2 restores the PL intensity, eventually plateauing at values close to those observed prior to exposure to O_2. The luminescence deactivation/re-activation observed when alternating between atmospheres of oxygen and nitrogen respectively suggests a reversible interaction with oxygen with **1** when dispersed in the pores of the SiO_2 matrix. In contrast, no PL quenching was seen when a simple powder of **1** was exposed to O_2. However, these data show that **1** can function successfully as a new O_2 sensor when loaded suitably in a porous matrix [41,63,45]. As reported earlier the hybrid material based on organic-metal complexes have multiple sensory functions with good efficiency and consequently increasing the variety of functional materials for technological applications in recent times [3-5].

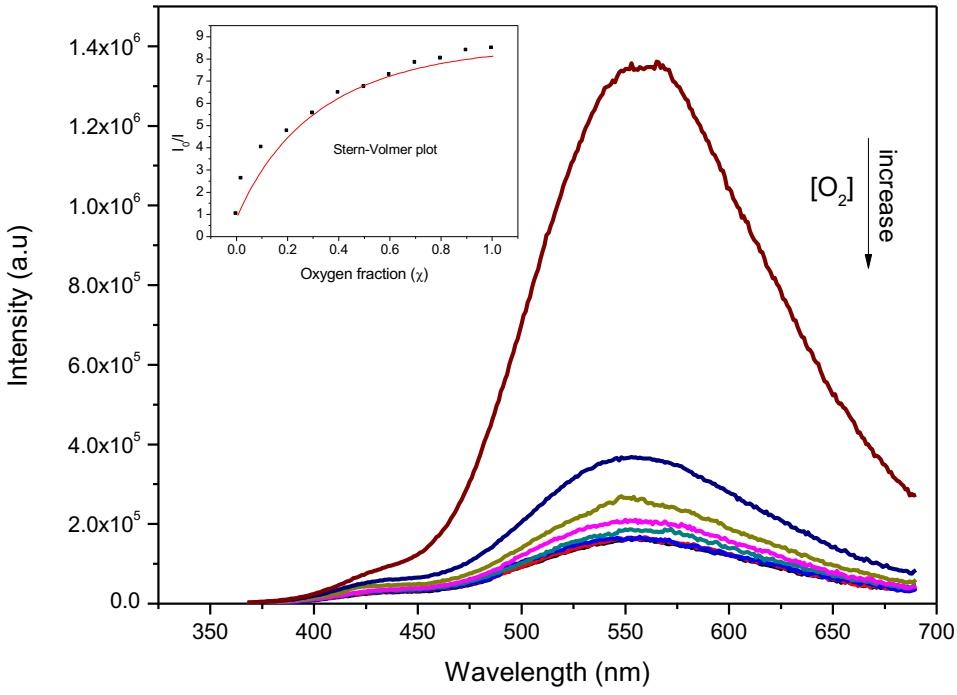

Figure 10. Emission spectrum for sample **1**@SiO_2 (λ_{exc} = 350 nm) with luminescence quenching as a function of oxygen concentration. inset: Plot of I_o/I as function of oxygen molar fraction (χ).

The insert appearing in Figure 10 is a plot of I_o/I vs χ_{O2} for the emission from **1**@SiO_2 as a function of increasing O_2 mole fraction in nitrogen. Inspection of this plot shows that it does not display the linear relationship predicted by the Stern-Volmer equation: $I_0/I = 1 + K_{SV}\chi_{O2}$, where I_o and I are the luminescence intensities in the absence and presence of the O_2 quencher, respectively, It has been hypothesized that such a deviation from linear behavior is a consequence of the heterogeneous environment where localized sites which can alter the linear quenching behavior [22,23,41,63].

In this context, we will consider Eq. 1 which models the mechanism for quenching at two principal sites within the matrix with different accessibility to oxygen:

$$\frac{I_o}{I} = \frac{1}{\frac{S_1}{1 + K_{sv}^1 \chi O_2} + \frac{S_2}{1 + K_{sv}^2 \chi O_2}} \qquad (1)$$

where S_1 and S_2 are the fractional contributions of each site ($S_1 + S_2 = 1$) and K^1_{sv} and K^2_{sv} are Stern-Volmer constant for each site [23,41,63,64]. This gives the better fit shown in Figure 10 with $K^1_{sv} = 28$ and $K^2_{sv} = 0.012$ with $R^2 = 0.967$, suggesting that the first site is easily accessible to oxygen, while the second site is not [65]. Since the curve fit is far from perfect there may be interplay with other PL quenching processes.

4. CONCLUSIONS

The color change of compound **1** when it is recrystallized from acetonitrile is a reversible process caused by a distorted molecular packaging in the solid state. These distortions also altered the photophysical properties of the complex, namely a blue shift of the PL spectrum and a somewhat longer lifetime. The solvatochromic effect was confirmed by shifting the absorption spectrum UV-Visible absorption spectrum to the blue as a function of increased polarity solvent. When **1** was incorporated into a silica mesoporous matrix there was a major shift of the PL band to the blue, consistent with a strong rigidochromic effect with color change. The PL of the resulting material was subject to quenching by oxygen. The non-linear relationship between I_o/I and χ_{O2} indicates that **1**@SiO_2 has multiple luminescent sites with different accessibility to

oxygen. The functionalities of this new copper (I) mononuclear complex, especially when incorporated in mesoporous silica, demonstrate its potential for applications in gas sensors, and other devices.

ASSOCIATED CONTENT

Supporting Information

AUTHOR INFORMATION

Corresponding Authors

*L.P.R.: e-mail, ravaro@ifsc.usp.br

*A.S.S.C.: e-mail, andreasc@ifsc.usp.br

ACKNOWLEDGEMENTS

Authors would like to thank Dr. Alexander Mikhailovsky, from UC Santa Barbara, for the lifetime measurements. Financial support from the Brazilian funding agencies FAPESP – São Paulo Research Fundation (2013/07793-6 (A. S. S. C.) CNPQ – Conselho Nacional de Desenvolvimento Científico e Tecnológico is also greatly appreciated. L. P. R. is personally thankful to FAPESP for a postdoctoral fellowship (2016/17495-0 and 2013/24727-7). Research at UCSB was partially supported by a grant from the US National Science Foundation (CHE-1565702).

References

[1] Penney AA, Sizov VV, Grachova EV, Krupenya DV, Gurzhiy VV, Starova GL, Tunik SP. Aurophilicity in Action: Fine-tuning the Gold(I)−Gold(I) distance in the excited state to modulate the emission in a series of dinuclear homoleptic Gold(I)−NHC complexes. Inorg Chem 2016; 55: 4720-4732.

[2] Wang X, Li Y, Wang L, Zhang J. Theoretical studies on cyclometalated platinum(II) complexes based on isoquinolinyl azolate: $\pi\pi$-stacking interaction and photophysical properties. Orga Electron 2016; 35: 208-215.

[3] Gao R, Zhao Y, Yang X, Yan D. Stimuli-responsive fluorescence based on the solid-state bis[2-(2-benzothiazoly)phenolato] zinc(II) complex and its fiber thin film. RSC Adv 2015; 2015, 5: 56470-56477.

[4] Yang X, Yan D. Long-afterglow metal–organic frameworks: reversible guest-induced phosphorescence tenability. Chem Sci 2016; 7: 4519–4526.

[5] Yang X, Yan D. Strongly Enhanced Long-Lived Persistent Room Temperature Phosphorescence Based on the Formation of Metal–Organic Hybrids. Adv Opt Mater 2016; 4: 897–905.

[6] Cariati E, Lucenti E, Botta C, Giovanella U, Marinotto D, Righetto S. Cu(I) hybrid inorganic–organic materials with intriguing stimuli responsive and optoelectronic properties. Coord Chem Rev 2016; 306: 566-614.

[7] Zink DM, Bachle M, Baumann T, Nieger M, Kühn M, Wang C, Klopper W, Monkowius U, Hofbeck T, Yersin H, Brasë S. Synthesis, Structure, and Characterization of Dinuclear Copper(I) Halide Complexes with P^N Ligands Featuring Exciting Photoluminescence Properties. Inorg Chem 2013; 52: 2292-2305.

[8] Ford PC, Vogler A. Photochemical and Photophysical Properties of Tetranuclear and Hexanuclear Clusters of Metals with d^{10} and s^2 Electronic Configurations. Acct Chem Res 1993; 26: 220-226.

[9] Ford PC, Cariati E, Bourassa J. Photoluminescence Properties of Multinuclear Copper(I) Compounds. Chem Rev 1999; 99: 3625-3647.

[10] Chen JL, Fu XF, Wang JY, Guo ZH, Xiao YL, He LH, Wen HR. A series of new emissive mononuclear copper(I) bipyridyl complexes bearing the methoxycarbonyl groups. Inorg Chem Comm 2015; 53: 88-91.

[11] Zigler DF, Tordin E, Wu G, Iretskii A, Cariati E, Ford PC. Mononuclear copper(I) complexes of O-t-butyl-1,1-dithiooxalate and of O-t-butyl-1-perthio-1-thiooxalate. Inorg Chim Acta 2011; 374: 261-268.

[12] Volz D, Baumann T, Flügge H, Mydlak M, Grab T, Bächle M, Barner-Kowollik C, Bräse S. Auto-catalysed crosslinking for next-generation OLED-design. J Mater Chem 2012; 22: 20786-20790.

[13] Dumur F. Recent advances in organic light-emitting devices comprising copper complexes: A realistic approach for low-cost and highly emissive devices?. Org Electron 2015; 21: 27-39.

[14] Yersin H. Highly Efficient OLEDs with Phosphorescent Materials; Wiley-VCH: Weinheim, Germany, 2008.

[15] Zhang F, Guan Y, Chen X, Wang S, Liang D, Feng Y, Chen S, Li S, Li Z, Zhang F, Lu C, Cao G, Zhai B. Syntheses, Photoluminescence, and Electroluminescence of a Series of Sublimable Bipolar Cationic Cuprous Complexes with Thermally Activated Delayed Fluorescence. Inorg Chem 2017; 56: 3742-3753.

[16] Zhao W, Montgomery J. Cascade Copper-Catalyzed 1,2,3-Trifunctionalization of Terminal Allenes. J Am Chem Soc 2016; 138: 9763-9766.

[17] Feldman RA, Fraile JM. Non-covalent immobilization of chiral copper complexes on Al-MCM41: Effect of the nature of the ligand. Catal Commun 2016; 83: 74-77.

[18] Zhan G, Zhong W, Wei Z, Liu Z, Liu X. Roles of phenol groups and auxiliary ligand of copper(II) complexes with tetradentate ligands in the aerobic oxidation of benzyl alcohol. Dalton Trans 2017; 46: 8286-8297.

[19] Ma DL, He HZ, Leung KH, Chan DSH, Leung CH. Bioactive Luminescent Transition-Metal Complexes for Biomedical Applications. Angew Chem Int Ed 2013; 52: 7666-7682.

[20] Gai Y, Sun L, Hui W, Ouyang Q, Anderson CJ, Xiang G, Ma X, Zeng D. New Bifunctional Chelator *p*-SCN-PhPr-NE3TA for Copper-64: Synthesis, Peptidomimetic Conjugation, Radiolabeling, and Evaluation for PET Imaging. Inorg Chem 2016; 55: 6892-6901.

[21] Fazaeli Y, Feizi S, RJalilian A, Hejrani A. Graftingof [^{64}Cu]-TPPF20 porphyrin complex on Functionalized nano-porous MCM-41 silica as a potential cancer imaging agent. Appl Radiat Isot 2016; 112: 13-19.

[22] Guangying L, Jun F. A series of phosphorescent Cu(I) complexes: Synthesis, photophysical feature and optical oxygen sensing performance in MCM-41 silica matrix. Sens Actuator B-Chem 2016; 233: 347-354.

[23] Smith CS, Branham CW, Marquardt BJ, Mann KR. Oxygen Gas Sensing by Luminescence Quenching in Crystals of Cu(xantphos)(phen)+ Complexes. J Am Chem Soc 2010; 132: 14079-14085.

[24] Lane AC, Vollmer MV, Laber CH, Melgarejo DY, Chiarella GM, Fackler JP, Yang X, Baker GA, Walensky JR. Multinuclear Copper(I) and Silver(I) Amidinate Complexes: Synthesis, Luminescence, and CS_2 Insertion Reactivity. Inorg Chem 2014; 53: 11357-11366.

[25] Wanga L, Wanga Z, Xianga Q, Chena Y, Duana Z, Xu J. High performance formaldehyde detection based on a novel copper (II) complex functionalized QCM gas sensor. Sens Actuators B Chem 2017; 248: 820-828.

[26] Kui SCF, Chui SSY, Che CM, Zhu N. Structures, Photoluminescence, and Reversible Vapoluminescence Properties of Neutral Platinum(II) Complexes Containing Extended π-Conjugated Cyclometalated Ligands. J Am Chem Soc 2006; 128: 8297-8309.

[27] Bencini A, Casarin M, Forrer D, Franco L, Garau F, Masciocchi N, Pandolfo L, Pettinari C, Ruzzi M, Vittadini A. Magnetic Properties and Vapochromic Reversible Guest-Induced Transformation in a Bispyrazolato Copper(II) Polymer: an Experimental

and Dispersion-Corrected Density Functional Theory Study. Inorg Chem 2009; 48: 4044-4051.

[28] Bailey RC, Hupp JT. Large-Scale Resonance Amplification of Optical Sensing of Volatile Compounds with Chemoresponsive Visible-Region Diffraction Gratings. J Am Chem Soc 2002; 124: 6767-6774.

[29] Ohara H, Ogawa T, Yoshida M, Kobayashi A, Kato M. Reversible luminescent colour changes of mononuclear copper(I) complexes based on ligand exchange reactions by N-heteroaromatic vapours. Dalton Trans 2017; 46: 3755-3760.

[30] Yam VWW, Wong KMC, Zhu N. Solvent-Induced Aggregation through Metal···Metal/π···π Interactions: Large Solvatochromism of Luminescent Organoplatinum(II) Terpyridyl Complexes. J Am Chem Soc 2002; 124: 6506-6507.

[31] Dias HVR, Diyabalanage HVK, Rawashdeh-Omary MA, Franzman MA, Omary MA. Bright Phosphorescence of a Trinuclear Copper(I) Complex: Luminescence Thermochromism, Solvatochromism, and "Concentration Luminochromism". J Am Chem Soc 2003; 125: 12072-12073.

[32] Vickery JC, Olmstead MM, Fung EY, Balch AL. Solvent-Stimulated Luminescence from the Supramolecular Aggregation of a Trinuclear Gold(I) Complex that Displays Extensive Intermolecular Au ···Au Interactions. Angew Chem Int Ed Engl 1997; 36: 1179-1181.

[33] Buss CE, Mann KR. Synthesis and Characterization of $Pt(CN\text{-}p\text{-}(C_2H_5)C_6H_4)_2(CN)_2$, a Crystalline Vapoluminescent Compound That Detects Vapor-Phase Aromatic Hydrocarbons. J Am Chem Soc 2002; 124: 1031-1039.

[34] Grove LJ, Rennekamp JM, Jude H, Connick WB. A New Class of Platinum(II) Vapochromic Salts. J Am Chem Soc 2004; 126: 1594-1595.

[35] Ni J, Wu YH, Zhang X, Li B, Zhang LY, Chen ZN. Luminescence Vapochromism of a Platinum(II) Complex for Detection of Low Molecular Weight Halohydrocarbon. Inorg Chem 2009; 48: 10202-10210.

[36] Cariati E, Bourassa J, Ford PC. Luminescence response of the solid state polynuclear copper(I) iodide materials $[CuI(4\text{-picoline})]_x$ to volatile organic compounds. Chem Commun 1998; 16: 1623-1624.

[37] Cariati E, Bu X, Ford PC. Solvent- and Vapor-Induced Isomerization between the Luminescent Solids $[CuI(4\text{-pic})]_4$ and $[CuI(4\text{-pic})]_\infty$ (pic = methylpyridine). The Structural Basis for the Observed Luminescence Vapochromism. Chem Mater 2000; 12: 3385-3391.

[38] Zhang R, Liang Z, Han A, Wu H, Du P, Lai W, Cao R. Structural, spectroscopic and theoretical studies of a vapochromic platinum(II) terpyridyl complex. CrystEngComm 2014; 16: 5531-5542.

[39] Wenger OS. Vapochromism in Organometallic and Coordination Complexes: Chemical Sensors for Volatile Organic Compounds. Chem Rev 2013; 113: 3686-3733.

[40] Po C, Tam AYY, Wong KMC, Yam VWW. Supramolecular Self-Assembly of Amphiphilic Anionic Platinum(II) Complexes: A Correlation between Spectroscopic and Morphological Properties. J Am Chem Soc 2011; 133: 12136-12143.

[41] Kato M, Omura A, Toshikawa A, Kishi S, Sugimoto Y. Vapor-Induced Luminescence Switching in Crystals of the Syn Isomer of a Dinuclear (Bipyridine)platinum(II) Complex Bridged with Pyridine-2-Thiolate Ions. Angew Chem Int Ed 2002; 41: 3183-3185.

[42] Quaranta M, Borisov SM, Klimant I. Indicators for optical oxygen sensors. Bioanal Rev 2012; 4: 115-157.

[43] Smith CS, Mann KR. Exceptionally Long-Lived Luminescence from $[Cu(I)(isocyanide)_2(phen)]^+$ Complexes in Nanoporous Crystals Enables Remarkable Oxygen Gas Sensing. J Am Chem Soc 2012; 134: 8786-8789.

[44] McGee KA, Veltkamp DJ, Marquardt BJ, Mann KR. Porous Crystalline Ruthenium Complexes Are Oxygen Sensors. J Am Chem Soc 2007; 129: 15092-15093.

[45] Ravaro LP, Almeida TR, Albuquerque RQ, Camargo ASS. The polynuclear complex $Cu_4I_4py_4$ loaded in mesoporous silica: photophysics, theoretical investigation, and highly sensitive oxygen sensing application. Dalton Trans 2016; 45: 17652-17661.

[46] Watts RJ, Missimer D. Environmentally Hindered Radiationless Transitions between States of Different Orbital Parentage in Iridium (III) Complexes. Application of Rigid-Matrix Induced Perturbations of the Pseudo-Jahn-Teller Potential to the Rigidochromic Effect in d6 Metal Complexes. J A Chem Soc 1978; 16: 5350-5357.

[47] Kotch TG, Lees AJ, Fuerniss SJ, Papathomas KI, Snyder RW. Luminescence rigidochromism of fac-tricarbonylchloro(4,7-diphenyl-1,10-phenanthroline)rhenium as a spectroscopic probe in monitoring polymerization of photosensitive thin films. Inorg Chem 1993; 32: 2570-2575.

[48] Itokazu MK, Polo AS, Iha NYM. Luminescent rigidochromism of fac-$[Re(CO)_3(phen)(cis\text{-}bpe)]^+$ and its binuclear complex as photosensors. J Photochem Photobiol A Chem 2003; 160: 27-32.

[49] Giordano PJ, Wrighton, MS. The nature of the lowest excited state in fac-tricarbonylhalobis(4-phenylpyridine)rhenium(I) and fac-tricarbonylhalobis(4,4'-bipyridine)rhenium(I): emissive organometallic complexes in fluid solution. J A Chem Soc 1979; 23: 2888-2897.

[50] Becker W. Advanced time-correlated single-photon counting techniques. Springer, Berlin, Heidelberg, New York, 2005

[51] Reichardt C. Solvatochromism, Thermochromism, Piezochromism, Halochromism, and Chiro-Solvatochromism of Pyridin ium *N*- Phenoxide Betaine Dyes. Chem Soc Rev 1992; 147-153.

[52] Reichardt C. Solvatochromic Dyes as Solvent Polarity Indicators. Chem Rev 1994; 94: 2319-2358.

[53] Gneuß T, Leitl MJ, Finger LH, Yersin H, Sundermeyer J. A new class of deep-blue emitting Cu(I) compounds – effects of counter ions on the emission behavior. Dalton Trans 2015; 44: 20045-20055.

[54] Ohara H, Kobayashi A, Kato M. Simple and extremely efficient blue emitters based on mononuclear Cu(I)-halide complexes with delayed fluorescence. Dalton Trans 2014; 43: 17317-17323.

[55] Ohara H, Kobayashia A, Kato M. Effects of N-heteroaromatic ligands on highly luminescent mononuclear copper(I)–halide complexes. C R Chimie 2015; 18: 766-775.

[56] Leitl MJ, Küchle FR, Mayer HA, Wesemann L, Yersin H. Brightly Blue and Green Emitting Cu(I) Dimers for Singlet Harvesting in OLEDs. J Phys Chem A 2013; 117: 11823-11836.

[57] Araki H, Tsuge K, Sasaki Y, Ishizaka S, Kitamura N. Luminescence Ranging from Red to Blue: A Series of Copper(I)−Halide Complexes Having Rhombic $\{Cu_2(\mu\text{-}X)_2\}$ (X = Br and I) Units with N-Heteroaromatic Ligands. Inorg Chem 2005; 44: 9667-9675.

[58] Czerwieniec R, Yersin H. Diversity of Copper(I) Complexes Showing Thermally Activated Delayed Fluorescence: Basic Photophysical Analysis. Inorg Chem 2015; 54: 4322−4327.

[59] Czerwieniec R, Leitl MJ, Homeier HHH, Yersin H. Cu(I) complexes – Thermally activated delayed fluorescence. Photophysical approach and material design. Coord Chem Rev 2016; 325: 2-28.

[60] Bizzarri C, Hundemer F, Busch J, Bräse S. Triplet emitters versus TADF emitters in OLEDs: A comparative study. Polyhedron 2018; 140: 51–66.

[61] Yersin H, Rausch AF, Czerwieniec R, Hofbeck T, Fischer T. The triplet state of organo-transition metal compounds. Triplet harvesting and singlet harvesting for efficient OLEDs. Coord Chem Rev 2011; 255: 2622– 2652.

[62] Zhang F, Guan Y, Chen X, Wang S, Liang D, Feng Y, Chen S, Li S, Li Z, Zhang F, Lu C, Cao G, Zhai B. Syntheses, Photoluminescence, and Electroluminescence of a Series of

Sublimable Bipolar Cationic Cuprous Complexes with Thermally Activated Delayed Fluorescence. Inorg Chem 2017; 56: 3742−3753.

[63] Yang X, Li Y. Construction and O_2 sensing performance of a core–shell structured magnetic-mesoporous composite functionalized with a ruthenium complex. Microporous and Mesoporous Mater 2015; 215: 84-90.

[64] Lei BF, Li B, Zhang HR, Lu SZ, Zheng ZH, Li WL, Wang Y. Mesostructured Silica Chemically Doped with RuII as a Superior Optical Oxygen Sensor. Adv Funct Mater 2006; 16: 1883-1891.

[65] Carraway ER, Demas JN, DeGraff BA, Bacon JR. Photophysics and photochemistry of oxygen sensors based on luminescent transition-metal complexes. Anal Chem 1991; 63: 337-342.

TOC